Jestr

Journal of Engineering Science and Technology Review 14 (6) (2021) 55 - 67

JOURNAL OF
Engineering Science and Technology Review

Research Article

www.jestr.org

Experimental Study on the Bending Behavior of Timber-steel Composite Box Beams

Yun Lei, Jiejun Wang*, Jiatong Liu and Ruiyue Liu

School of Civil Engineering, Central South University of Forestry and Technology, Changsha 410004, China

Received 30 July 2021; Accepted 11 December 2021

Abstract

The mechanical properties of timber, a traditional green engineering material, are greatly affected by timber grain, thus limiting the application of timber structures in modern engineering. This study aimed to broaden the engineering application of timber structures and fully exploit the tensile and compressive properties of timber along the grain by proposing a box-section timber-steel composite beam with larch plywood as the upper and lower flanges and welding cold-formed thin-wall channel as the web, and these materials were connected using bolts. Three timber-steel composite box beams and one plywood box beam were separately subjected to bending loading tests by stepwise loading. For the composite and plywood box beams, mechanical properties such as ultimate bending capacity and flexural stiffness were analyzed by observing the strain variation, deflection evolution, failure process, and shape of their flanges and webs under load effect. The shear lag coefficient and effective distribution width of the timber-steel composite box beam flanges were calculated according to the lateral flange strain distribution. Further, based on the computational formula of steel-concrete composite beams and considering the slip effect, the mid-span deflection and ultimate bearing capacity of the timber-steel composite box beams were quantitatively analyzed. Results show that the flanges and web of the composite box beams have good combination performance, and all the specimens undergo typical tensile and compressive failures accompanied by local buckling of steel and local splitting of timber. Plywood box beams are damaged via shear web failure along the grain. Steel web of composite box beams has better shear resistance than timber, subsequently, the ultimate bending capacity of the composite box beams increase with an average of 30.3% compared to the plywood box beams, although the initial stiffness decrease by 34.8% on average. The calculations of the bearing capacity are in good agreement with the experimental results and meet the requirements of practical engineering applications. This study provides significantly references and new insights into widening the modern engineering application of timber structures.

Keywords: Timber-steel composite structure, box beam, plywood, steel plate, bending behavior, ultimate bearing capacity

1. Introduction

Timber is a green and renewable load-bearing structural material with the advantages of light weight, high strength, and good machinability. With increasing demand for environmental protection and the development of science and technology, the defects of traditional timber structures have been gradually overcome, the demand for engineering application of modern timber structures has grown prominently, and an increasing number of institutions and researchers has engaged in the application research of modern timber structures [1-2]. Related technologies have also made great progress.

However, timber is an anisotropic material, where the grain remarkably affects the mechanical properties. Its perpendicular-to-grain mechanical properties are considerably lower than its parallel-to-grain mechanical properties. Despite the high parallel-to-grain tensile and compressive strengths, the parallel-to-grain shear strength is low, making the timber structure prone to shear failure. This factor is also a major constraint to the engineering application of timber structures.

Based on the above analyses, composite structures formed by the combination of timber and other materials has become the focus of timber structure research, and extensive work has been made concerning the mechanical properties of timber-steel, timber-concrete, and other composite structures [3-5]. However, most studies focus on structures with rectangular or open sections, such as T- and I-shaped sections. Box sections are more advantageous over rectangular sections in terms of reasonable form and material saving, and they have better torsional performance than the T-shaped and other open sections. Therefore, they have been widely applied in the engineering field. However, box-section timber-steel composite beams have not been studied. Hence, timber-steel composite box beams should be studied, and their failure mechanism and bending bearing capacity should be determined to provide new perspective on the development of timber-steel composite structures.

Poor mechanical propertiy of timber beams limits engineering application, thus this study focused on timber-steel composite box beams connected by bolts to fully exploit the material performance and facilitate the utilization. . The webs of plywood box beams， which primarily bear shear stress, were replaced with steel. This configuration can improve the shear resistance of the box beams, thereby greatly improving the bearing capacity of the composite beams. The bending behavior of timber-steel composite box beams were explored through experimentation and theoretical analysis, and the findings can provide a reference for deeper research into the timber-steel composite structures.

*E-mail address: wangjiejun2011@126.com
ISSN: 1791-2377
doi:10.25103/jestr.146.06

2. State of the art

At present, scholars from all around the world have extensively studied timber-steel composite members and have made adequate progress. By comparing the mechanical properties between steel-timber and steel-concrete composite slabs of double-angle steel connecting beam-column joints, F. Nouri et al. [6] found that the steel-timber composite members have better rotational capacity and hogging moment resistance than steel-concrete ones. However, their results lacked universality because of the excessively small sample sizes for the same types of members. In terms of the connection behavior of beam-column joints, N. Keipour et al. [7] used different connection modes as variables to explore the mechanical properties of steel-timber composite beam-column joints through pushdown tests. The results showed that the beam-column joints had excellent hogging moment and rotational bearing capacities, although their overall deformation capacity was slightly reduced. By using compression tests, Ali Awaludin et al. [8] experimentally investigated the compression members of cold-formed steel-timber composite roof structures and found that the bearing capacity of composite members was significantly better than those of cold-formed steel members. they also summarized the formula for bearing capacity, although its application universality remains to be verified. Mark A. Bradford et al. [9] analyzed the slip behavior of lap joints for four different types of steel-timber composite joints after push-out tests. Results show that the plate nailing could improve the joint stiffness, although the joint strength was not substantially improved. Regarding the bearing capacity of steel-timber composite beams, A. Hassanieh et al. [10] made a bearing capacity comparison of steel-timber composite I-beams under different connection modes by experimentation combined with finite element analysis (FEA). Results show that the combination of glue and mechanical connections was conducive to improving the bearing capacity of members, although the durability problem of glue connection could not be well addressed in practical engineering. A. Hassanieh et al. [11-12] also experimentally analyzed the behavior of steel-timber composite connections and proposed an empirical load-slip formula based on non-linear regression. However, further studies were required to verify whether the empirical formula could reflect the experimental results accurately. By using cyclic loading tests, A. Ataei et al. [13] investigated the behavior of shear connectors of steel-timber composite beams under cyclic loading and found that the steel-timber composite joints had high ductility and energy dissipation capacity. Based on the test results, they introduced a simple hysteresis model, whose applicability to practical engineering remains unclear. By adopting different connection modes, Masanori Fujita et al. [14] explored the flexural behavior of timber beams embedded with I bars. However, large errors were recorded between the theoretical computations and experimental results of the bending capacity for the composite beams. Junren Wang et al. [15] conducted compression tests on H-shaped steel-timber composite columns and analyzed the effects of connection mode on the bearing capacity and stability of the composite columns. Jiejun Wang et al. [16] experimentally compared the bending performance between steel-timber composite I-beams and plywood I-beams and found that the steel-timber composite I-beams had better bearing capacity than the plywood beams. However, they failed to summarize the computational formula of bearing capacity that conformed to the experimental results. Shaowei Duan et al. [17] enhanced the bearing capacity of composite beams by adding bolt anchors to the steel-timber composite beams and calculated the bearing capacity of composite beams according to the superposition principle. Regarding the shortcomings, the number of specimens was small, and the accuracy of theoretical bearing capacity calculation required further improvement. Gao Yimin [18] analyzed the CLT steel-timber composite bridge decks by using FEA method and summarized the simplified computational method of bearing capacity, whose feasibility in practical engineering application remains unclear. To explore the shear resistance of steel clamping plate bolted connections for pre-fabricated timber structures, Chen Aijun et al. [19] investigated the effects of shear failure mechanism and bolted gaskets of plywood-steel clamping plate bolted connections on their shear resistance by using push-out tests combined with FEA simulation. Results show that the gasket setting did not remarkably improve the bearing capacity. Chen Aiguo et al. [20] experimentally analyzed the flexural behavior of H-shaped steel-timber composite beams. Results show that despite the remarkably enhanced flexural stiffness and bearing capacity of the composite beams after timber reinforcement, the selection of variables that influence bearing capacity was limited. Yao Xuefeng[21] experimentally evaluated the mechanical properties of steel-timber composite beam bolted shear connectors and the bending resistance of steel-timber composite beams. However, considering the small data size, their conclusions require further validation.

The above studies focused on the mechanical properties of steel-timber composite beam-column joints and open section members. However, no scholars in China or other countries have explored the flexural behavior of box-section timber-steel composite beams, and a relevant design basis remains lacking for practical engineering applications. Therefore, the study employed a welded channel steel-timber composite box beam as the research object. The rationality of the composite box beam pattern was verified through comparative test with the plywood box beam. The flexural behavior of the composite box beam was investigated, and its failure modes and mechanisms were clarified. Further, the bearing capacity test results were compared with the corresponding theoretical calculations, thus providing reference for the popularization and application of timber-steel composite box beams in practical engineering.

The remainder of this study is organized as follows: In Section 3, the design and fabrication processes of the timber-steel composite and plywood box beam specimens and the bending loading test protocol are described. In Section 4, the mid-span deflection evolution, strain distribution, and timber-steel interface slip are tested, and the deflection and bearing capacity are calculated. The last section draws conclusions.

3. Methodology

3.1 Specimen design

For both the timber-steel composite beam and plywood box beam, the total length L was 1.8 m, and the calculated span L_0 was 1.52m. In the span direction of the plywood box beam, 20 mm-thick timber diaphragms were arranged at the loading point and support location. For composite box beam, 3 mm-thick steel diaphragms were arranged at the corresponding same locations. The upper and lower flanges

of the composite box beam were all plates made of pine sawn timber, whereas the webs were Q235 channel steel, and they were connected by bolts. The plywood box beam was made by laminating timber boards. Figure 1 displays the design diagram of the specimens, where t_s , b_s , and h_w denote the thickness, leg width, and height of the channel steel (the leg thickness of channel steel was the same as its waist thickness), b_1 and b_2 denote the upper and lower flange plate widths, respectively, t represents the plate thickness (in the plywood box beam, the web was equal in thickness to the flange plate), and *h* represents the total height of the box beam. The channel steel was placed upright, in which the leg ends were parallel to and at the same level with the sides of lower flange plate. The plywood box beam specimen was numbered L0, while the timber-steel composite box beam specimens were numbered L1~L3.

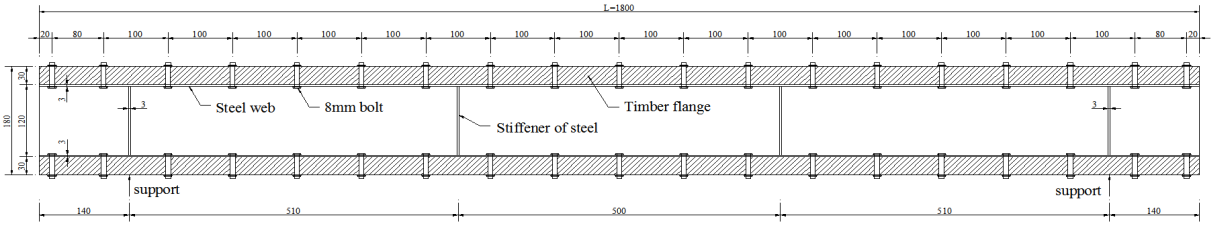

(a) Longitudinal section of composite box beam

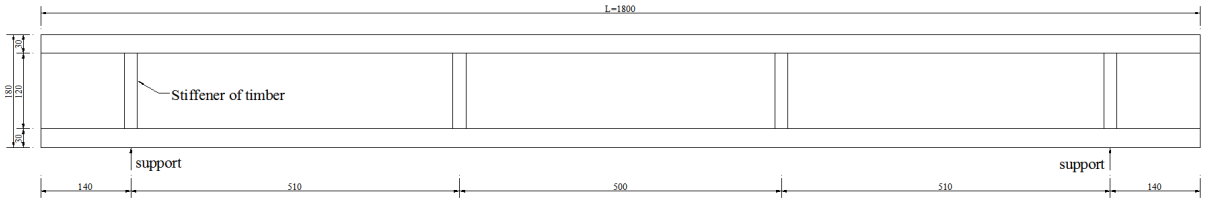

(b) Longitudinal section of plywood box beam

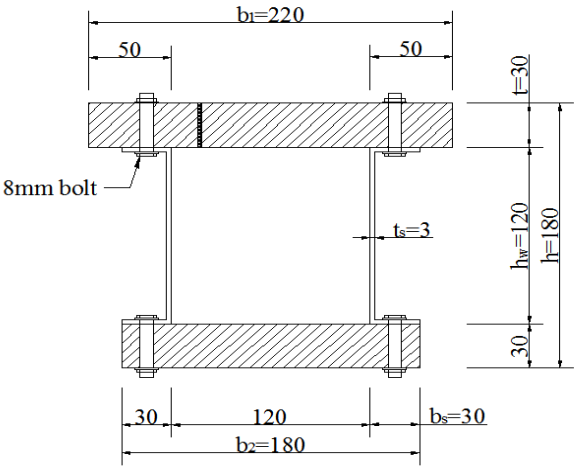

(c) Cross section of composite box beam

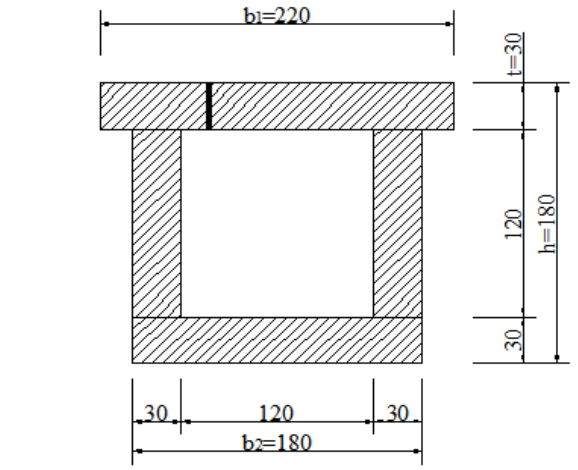

(d) Cross section of plywood box beam

Fig.1. Specimen design diagrams (unit: mm)

3.2 Material property parameters

Larix gmelinii was used as the timber, and its material properties were tested in the laboratory of the School of Materials Engineering, Central South University of Forestry and Technology. Small clear timber specimens were fabricated, and their parallel-to-grain shear, compressive, and tensile strengths were measured. The test results were reduced as per the Design Handbook for Timber Structures [22], and the final results are summarized in Table 1. The channel steel was welded and machined from Q235 steel, and Table 2 summarizes the mechanical property data of the steel. The bolts used were M8 grade 4.8 bolts with hexagonal heads, whose arrangement conformed to the requirements of relevant standards.

Table 1. Mechanical properties of timber

Moisture content (%)	Parallel-to-grain compressive strength (MPa)	Parallel-to-grain tensile strength (MPa)	Parallel-to-grain shear strength (MPa)	Elastic modulus (MPa)
13.6	26	103	7	12,230

Table 2. Mechanical properties of steel

Yield strength (MPa)	Tensile strength (MPa)	Shear strength (MPa)	Elastic modulus (GPa)
235	375	141	206

3.3 Loading device and measuring point arrangement

The tests were conducted under a 100-t reaction frame in the Structural Laboratory of Central South University of Forestry and Technology, and the load measurement was accomplished with 30-t load sensor. Four-point bending loading was employed, and Figure 2 illustrates the loading device arrangement. Manual stepwise loading was adopted, where at loads less than 80 kN, the load increment at each step was 10 kN; at loads greater than 80 kN but less than 120 kN, the load increment at each step was 5 kN; and when

the load exceeded 120 kN, the load increment at each step was 2 kN until the members could no longer bear the load.

During specimen loading, the readings of strain gauges and displacement sensors were all collected synchronously by using the DH3861 static strain acquisition system. For the arrangement protocol of measurement points, two displacement sensors (readings were averaged) were arranged at the bottom surface of mid-span position for each specimen to measure the vertical deflection of mid-span section. One displacement sensor was arranged at the interface between beam end timber and steel of the composite beams to measure the relative timber-steel slip, that is, the relative dislocation between timber and steel caused by the gradual failure of shear connectors in the loading process. Five strain gauges were evenly arranged at the top and bottom surfaces of mid-span section for each member. One strain gauge was arranged at the bottom surface of upper flange for each composite beam. At the composite beam side surfaces, three strain gauges were evenly arranged at the web part, one strain gauge was arranged at the upper flange, and two strain gauges were arranged at the lower flange. For the plywood box beam, six strain gauges were arranged on its side surfaces. The two sides were arranged symmetrically, and Figure 3 depicts the measuring point arrangement. In the present tests, the mid-span deflection, strain of mid-span section, ultimate load, and relative slip of timber-steel interface were measured for each specimen.

Fig.2. Photo of loading device

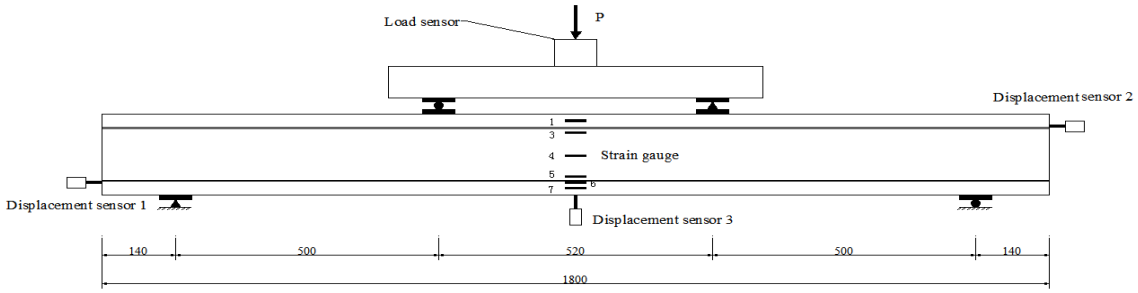

(a) Schematic of loading arrangement

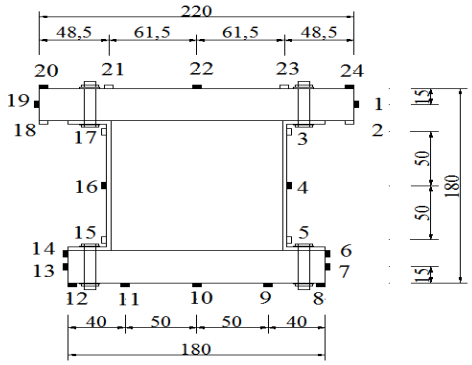

(b) Measurement point arrangement of composite beam mid-span section

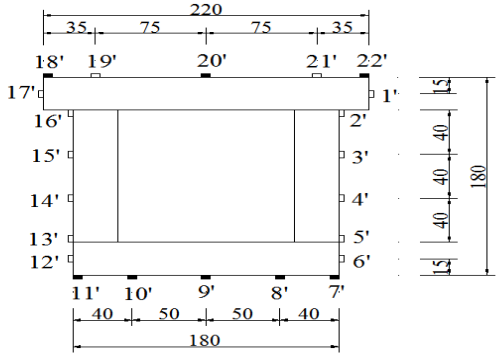

(c) Measurement point arrangement of timber beam mid-span section

Fig.3. Schematics of specimen loading and measurement point arrangements (unit: mm)

4 Result Analysis and Discussion

4.1 Analysis of failure modes

Figure 4 displays the failure modes of various specimens. As shown in Figure 4(a), the plywood box beam typically failed through shear cracks in the middle of the web. This phenomenon can be attributed to the considerably higher parallel-to-grain tensile and compressive strengths of timber than its shear strength. Before the normal stress of flanges reached the tensile and compressive strengths of timber, the shear stress of web already reached the parallel-to-grain shear strength of timber, immediately after which shear failure occurred. Considering that the highest shear stress of section occurred near the central axis, initial shear crack was generated in the middle of web. With further increase of load, the initial crack continued to extend and penetrate along the longitudinal direction of specimen, eventually extending to the beam ends. At this point, the plywood box beam was damaged because of the loss of bearing capacity. Local longitudinal cracks were observed on the top surface of upper flange for the plywood box beam (Figure 4b). This phenomenon can be attributed to the presence of original defects such as wood knots in the timber, where original fine cracks are prone to appear. When the local force near the loading point was excessively large, the original cracks continuously extended and eventually developed into coherent local cracks. The plywood box beam underwent evident vertical deformation during the loading process, which recovered gradually after failure. Therefore, during damage, the plywood box beam did not enter the plastic stage as a whole. It lost its bearing capacity because of the

strength failure of some members, exhibiting the brittle failure feature.

For composite box beams, the typical failure mode was longitudinal tension-compression failure of flanges. The timber of lower flange was pulled and cracked, while the timber of upper flange was crumpled by compressive yielding. Meanwhile, accompanying the compressive yielding of upper web steel edge at the loading point, the upper flange also presented with apparent local splitting, as shown in Figures 4(d)-4(l). Considering that steel with high shear strength was used for the webs of composite beams, they did not undergo shear failure. Instead, the upper edges of the steel webs were buckled because of excessive compressive stress at the middle and later stages of loading. The section pattern of the present specimens was up-down asymmetric, with the neutral axis being over half of the section height (h/2: 90mm, distance of center axis from beam bottom: approximately 106mm). Subsequently, the tensile stress of lower flange was greater than that of upper flange for the composite beams. When the maximum tensile stress exceeded the ultimate tensile strength of timber, the timber was pulled to failure, and initial cracks formed. As the loading increased, the initial cracks gradually extended and penetrated into the lateral direction, leading to failure of the composite beams caused by the loss of bearing capacity. During failure, the timber of upper flange was also crumpled because of compressive yielding , suggesting that the composite box beams gave full play to the material performance. The local longitudinal cracks on the flanges were attributable to the effect of shear lag. All the composite box beams underwent evident vertical deformation by the action of vertical concentrated load, from which recovery is not possible after the specimen failure. Suggestively, the composite beams already entered the plastic stage and had good ductility.

(a) Shear crack in the middle of beam L0 web

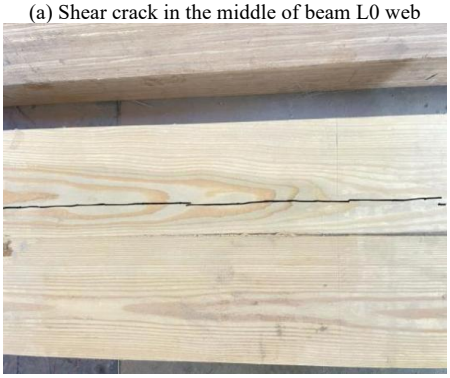

(b) Local longitudinal crack on beam L0 top surface

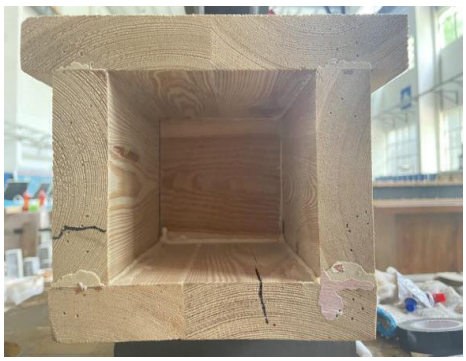

(c) Cracks on beam L0 end

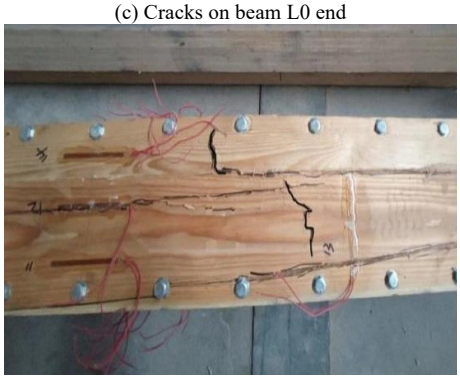

(d) Parallel-to-grain tensile cracking of timber on beam L1 bottom surface

(e) Parallel-to-grain buckling and local splitting of timber on beam L1 top surface

(f) Buckling of beam L1 steel web upper exterior

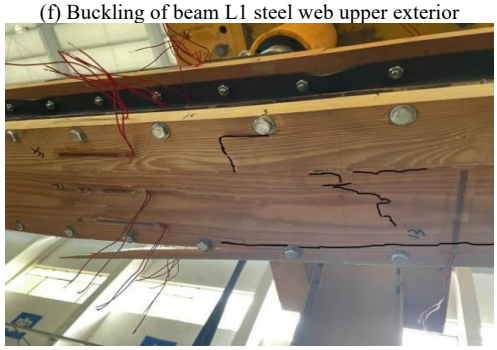

(g) Parallel-to-grain tensile cracking of timber on beam L2 bottom plate

(h) Parallel-to-grain buckling and local splitting of timber on beam L2 top surface

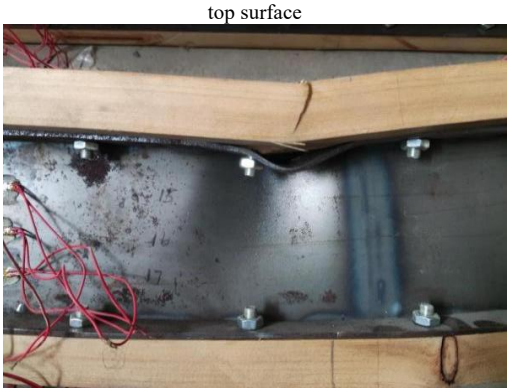

(i) Buckling of beam L2 steel web upper exterior

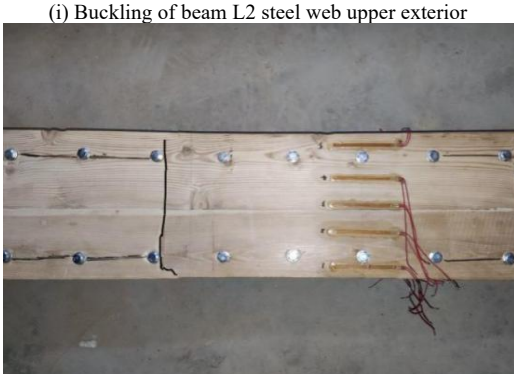

(j) Parallel-to-grain buckling and local splitting of timber on beam L3 top surface

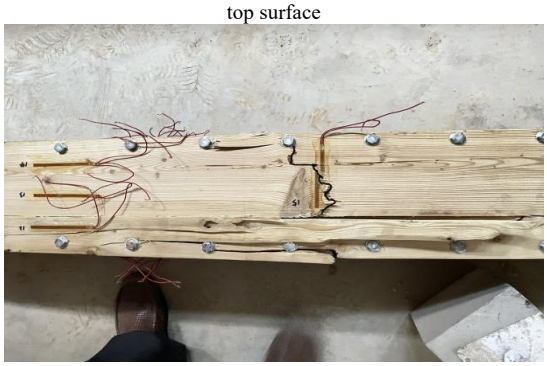

(k) Parallel-to-grain tensile cracking of timber on beam L3 bottom surface

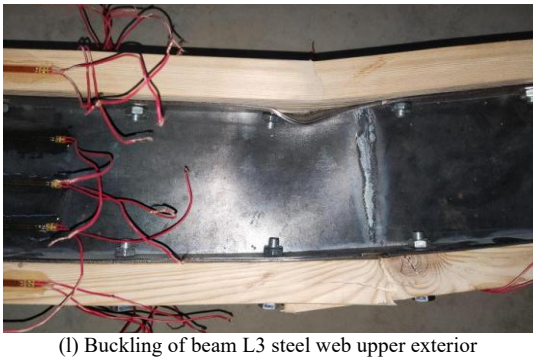

(l) Buckling of beam L3 steel web upper exterior

Fig. 4. Failure modes of specimens

4.2 Load-mid-span deflection curves

Figure 6 displays the load–mid-span deflection curves of four specimens. The slope of load–deflection curve for the line connecting two points (at 0.1 and 0.4 times of ultimate load) was defined as the initial stiffness of composite box beams as follows:

$$k = \frac{P_{0.4} - P_{0.1}}{\Delta_d} \tag{1}$$

where Δ_d denotes the difference between displacements corresponding to $P_{0.4}$ and $P_{0.1}$.

Yield point was defined based on the equivalent elastic–plastic yield design, as shown in Figure 5. Yield displacement was obtained from an elastic–plastic system, whose load–deflection curve had the same initial stiffness and ultimate strength values. Accordingly, the computational formula for specimen yield displacement Δ_y was as follows:

$$\Delta_y = \frac{P_u}{k} \tag{2}$$

The load corresponding to the yield displacement was precisely the yield load. Table 3 details the mechanical property data of specimens obtained based on the test results, where P_y, Δ_y, P_u, Δ_u and β denote the yield load, yield displacement, ultimate load, ultimate displacement, and ductility factor of specimens, respectively.

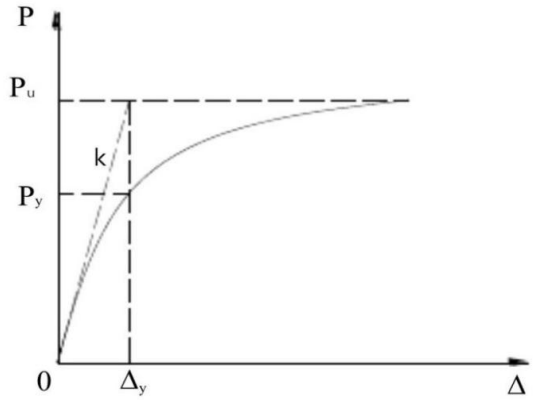

Fig. 5. Equivalent elastic–plastic yield curves

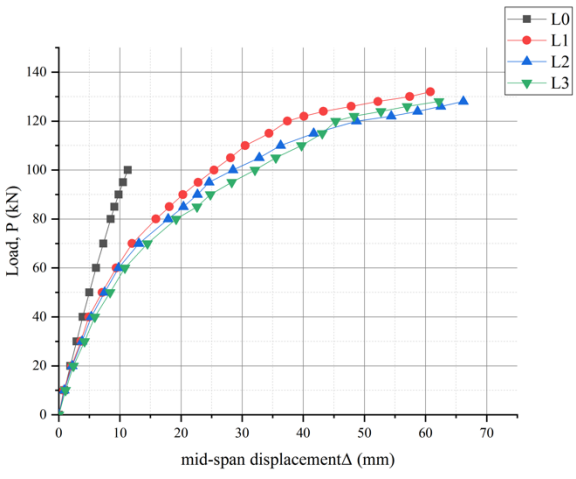

Fig. 6. Load–mid-span deflection curves

Table 3. Test data of specimen mechanical properties

Specimen	P_y (kN)	Δ_y (mm)	P_u (kN)	Δ_u (mm)	β	k (kN/mm)	R_{Pu}	R_k
L0	—	—	100	11.3	—	9.2	—	—
L1	93	20.6	132	60.8	2.95	6.4	32%	−30%
L2	87	21	128	66.2	3.15	6.1	28%	−34%
L3	87	23.4	131	61.2	2.62	5.6	31%	−39%
$\bar{L}$	88.7	21.7	130.3	62.7	2.91	6	30.3%	−34.8%

Note: $\bar{L}$ represents the average values of three composite box beams, R_{Pu} denotes the increase rate of ultimate bearing capacity for composite box beams compared with the plywood box beam with the formula of $R_{Pu}=\frac{P_{uLx}-P_{uL0}}{P_{uL0}}\times 100\%$ (P_{uLx} and P_{uL0} respectively represent the ultimate loads of composite and plywood box beams), and R_k represents the increase rate of initial stiffness, which is calculated similar to R_{Pu}.

As shown in Figure 6, the bearing capacities of composite box beams are all greater than those of plywood box beam, and the load–deflection curves of plywood box beam basically exhibit linear changes, resulting in brittle failure. In comparison with the plywood box beam, the ultimate bearing capacities of composite box beams increased by 30% on average, but the initial stiffness slightly declined. This phenomenon can be attributed to the glue connection between the web and flanges of plywood box beams, which achieved good integrity. By contrast, composite box beams were connected using bolts, leading to relative slip between wood boards and steel during the loading process and reducing the initial beam stiffness. Nevertheless, compared with the plywood box beam, which has brittle failure, the composite box beams show better ductility.

4.3 Strain analysis of mid-span sections

As shown in Figure 3, on the side surfaces of mid-span sections for the four specimens, strain gauges were arranged along the height. Figure 7 describes the height-dependent strain variations of mid-span sections for the four experimental beams under different load levels (data represent the average of two side surfaces). Based on the curves, the mid-span section strains of the plywood box beam L0 maintained an approximately linear distribution along the height under load action, suggesting that the plane section assumption was fundamentally satisfied. As shown in Figure 7(a), under the presence of overhang, the upper flange was affected by shear lag effect at the middle and later stages of loading and the strains on the upper flange sides are slightly smaller than those near the web. The specimens L1~L3 can fundamentally maintain linearity at low external loads. Considering that the web is replaced by welded channel steel, the distance of web exterior from flange exterior is far. Hence, the strain level of the web differs from that of the flanges. After the gradual failure of bolts at the middle and later stages of loading, such strain difference was further increased by the slip effect at the timber-steel interface. With the continuous increase in load, the relative slip between the flange timber and the web steel increased progressively upon gradual shear yielding of the bolts, and this condition drastically reduced the integrity of composite beams. At this point, the section strains of the entire composite beams no longer satisfy the plane section assumption, although the flange and web strains individually satisfy the plane section assumption. Finally, when the load approached ultimate load, the timber on the top surface of upper flange underwent compressive yielding. At this point, the timber strain in the compressive zone no longer satisfies the plane section assumption. Although the strain continued to increase, the load can no longer be increased, as shown in Figures 7 (b)-7(d).

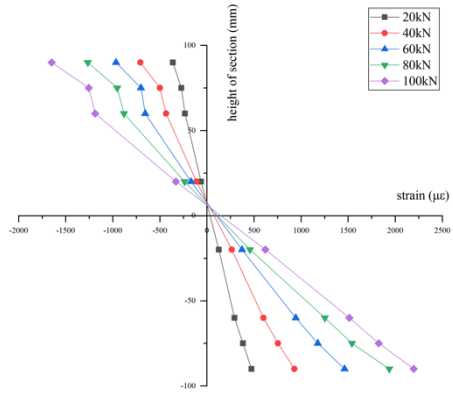

(a) Specimen L0

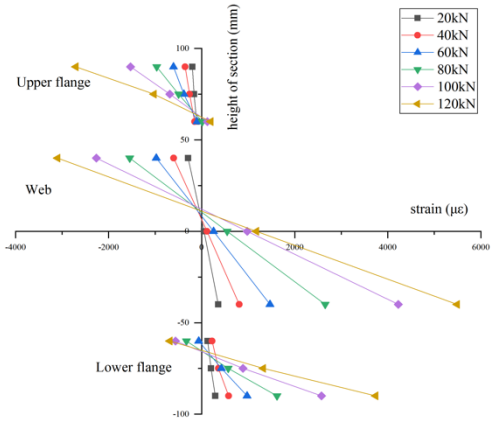

(b) Specimen L1

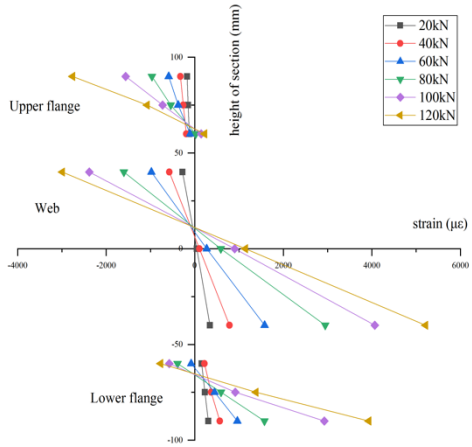

(c) Specimen L2

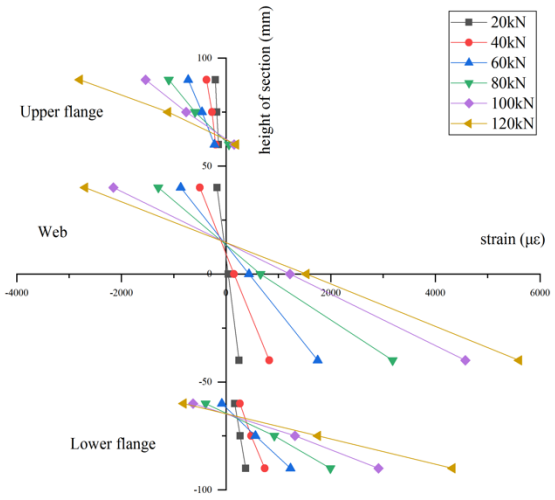

(d) Specimen L3

Fig. 7. Variation curves of mid-span strains along height

After extensive research it was found that timber undergoes an obvious yield stage under compression while presenting brittle failure under tension, and a tension–compression constitutive model was proposed. On this basis, Yang T, Li J et al. [1-2] further studied the wood properties and member stresses of larchwood. Based on the foregoing literature findings and the elastic moduli obtained from wood property test, this study calculated the yield compressive strain (2,301 με) and the ultimate tensile strain (8,422 με) of larchwood in the present tests. The curves indicate that when the load approached ultimate load, the top surface of upper flange timber already underwent compressive yielding. The measured maximum compressive strains of the three composite beams were 3,154, 3,281, and 3,283 με, respectively, which exceed the yield compressive strain of timber. At this point, the timber on the upper flange top surface already failed, and the neutral axis moved down. The maximum tensile strains of lower flange timber were 3,740, 3,933, and 4,328 με, which fail to reach the ultimate tensile strain of timber. Nevertheless, during the tests, the timber at the bottom was already cracked by tension, because the tensile properties of timber are unstable. The cracking and crack extension of timber during tensile brittle failure often result from the interaction between tensile and shear stresses, especially the perpendicular-to-grain tensile stress and parallel-to-grain shear stress [23]. The parallel-to-grain shear stress and perpendicular-to-grain tensile stress cause the tearing of the connections between wood fibers prior to tearing of the fibers themselves, thus reducing the area of the tensile zone, which has an amplifying effect on the tensile stress borne by wood fibers. Subsequently, the bottom plate timber undergoes tearing failure prior to reaching the ultimate tensile strain. The maximum tensile strains of steel measured in the tests are 5,492, 5,210 and 5,598 με, respectively, which exceed the steel yield strain. Suggestively, part of the steel already enters the yield stage when the composite beams are close to failure. Therefore, timber can exert its tensile and compressive behaviors, because the steel remedies its poor shear resistance.

4.4 Lateral distribution of flange strains

Ribbed section beams such as box beams generally have a shear lag effect. Under the action of bending moment, the normal stresses of box beam flanges are unevenly distributed along the lateral direction. In the present tests, five vertical strain gauges (Figures 3(b) and 3(c)) were evenly and laterally arranged on the top surface of upper flange at the mid-span position of each specimen to measure the lateral distribution of flange strains. Figure 8 displays the obtained lateral strain distribution curves of the upper flange top surface under various loads. At the initial stage of loading, the uneven distribution of lateral strains is unobvious. When the load exceeds 40% of the ultimate load, the flange strains near the web increase rapidly, while the strains far from the web increase rather gently. This phenomenon occurred, because the increased shear deformation of web leads to the deformation of flange near it, ultimately increasing the strain at this location.

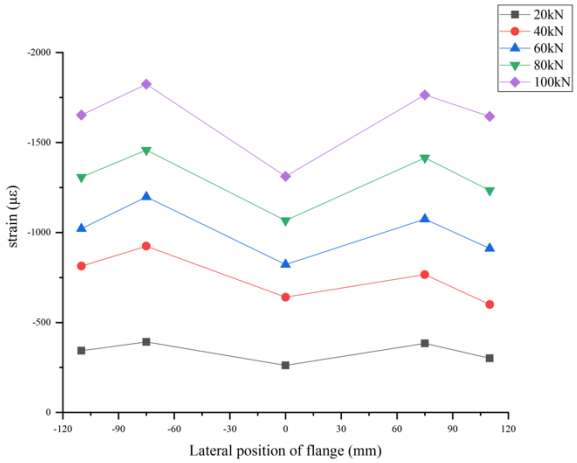

(a) Specimen L0

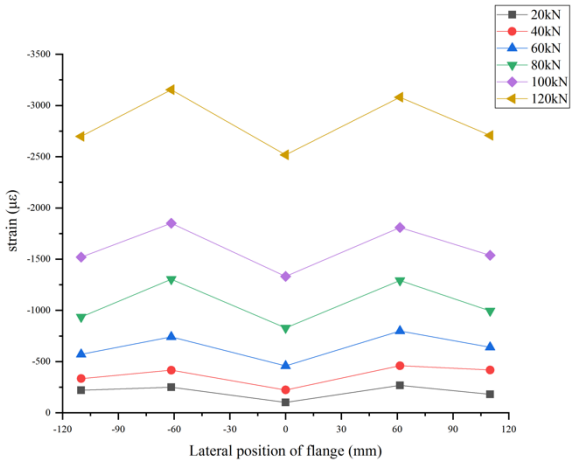

(b) Specimen L1

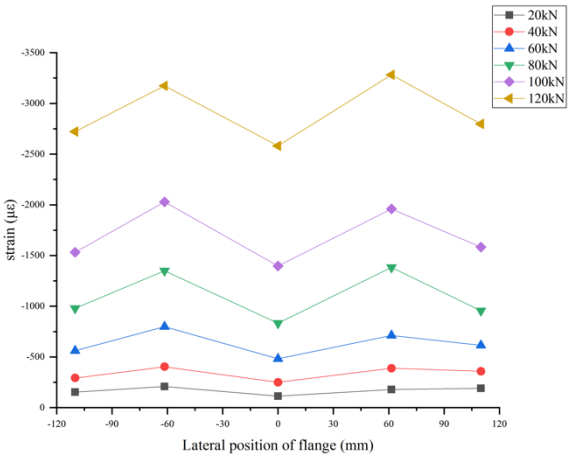

(c) Specimen L2

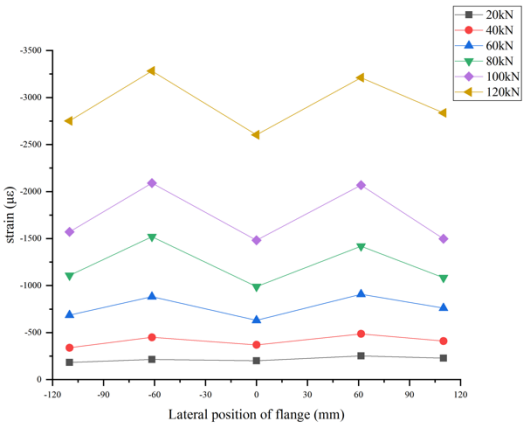

(d) Specimen L3

Fig. 8. Lateral distributions of box beam flange strains

The figure shows that the flange strains of the four specimens are all unevenly distributed in the lateral direction. The larger the position nears the web and the smaller the distance away from the web, the more evident the shear lags effect. The shear lag coefficient λ reflects the unevenness degree of the lateral distribution of flange normal stresses. Considering the practical engineering application and convenient determination of effective section width, the ratio of maximum to average stress of section is defined as the shear lag coefficient λ of the section as follows:

$$\lambda = \frac{\sigma_{max}}{\sigma_0} \tag{3}$$

where σ_{max} denotes the maximum normal stress at the flange, and σ_0 refers to the average normal stress of flange section obtained according to the elementary beam theory. Based on the approach of Xu Guo and Li Ping et al. [24-25], the calculation of σ_0 was simplified for the composite box beam flanges as follows:

$$\sigma_0 = \frac{\int_b \sigma dz}{b} \tag{4}$$

In the formula, b denotes the actual width of composite box beam flange.

The effective flange width is calculated using the following formula:

$$b_e = \frac{b\sigma_0}{\sigma_{max}} = \frac{b}{\lambda} \tag{5}$$

Based on the test results, the shear lag coefficient of upper flange at the mid-span position and the effective flange width were calculated for the four specimens, and the results are listed in Table 4. The shear lag coefficient of the plywood box beam is smaller than that of the composite box beams. This finding can be attributed to the thicker web and closer web wall to flange sides for the plywood box beam, which is thus less affected by the shear lag effect. By contrast, the webs of composite box beams are made of thinner steel, which are farther from the sides of flanges, resulting in obvious shear lag effect. Accordingly, the plywood box beam also exhibits larger effective flange width than the composite box beams.

Table 4. Shear lags coefficients and effective widths of upper flanges at the mid-span sections

Specimen	λ	b_e (mm)
L0	1.12	197.1
L1	1.15	191
L2	1.14	192.7
L3	1.15	191
$\bar{L}$	1.147	191.57

Note: $\bar{L}$ represents average values of three composite box beams.

4.5 Relative timber-steel slips of composite box beams

Considering that the deformation of shear connectors leads to the uncoordinated deformations of flange timber and web steel, relative slips are generated between the timber and the steel, thus reducing stiffness, increasing deflection, and decreasing the bending capacity of the composite box beams. Figure 9(a) presents the schematic diagram of relative timber-steel slips. To measure the relative slips between steel web and wood flange board of the composite beams, the displacement sensors at the beam ends are arranged and fixed on the steel web with magnetic base. The pointers of the displacement sensors are placed at the bottom end of wood board sides (timber-steel interface) to obtain the relative timber-steel slips. By using the steel as reference, the slip is regarded positive when the flange timber extends outwardly relative to the steel and regarded as negative when it shrinks inwardly relative to the steel. Figures 9(b)-9(c) describe the final slip phenomena at the beam ends for the L2 specimen. The resulting load-slip curves are presented in Figure 10. The maximum slips of the three specimens are all approximately 6 mm, while those at the two specimen ends are symmetrically distributed. The final slips at the left and right ends are basically the same for the three specimens, and those of upper flanges relative to steel are the same as those of lower flanges, albeit the opposite slip directions.

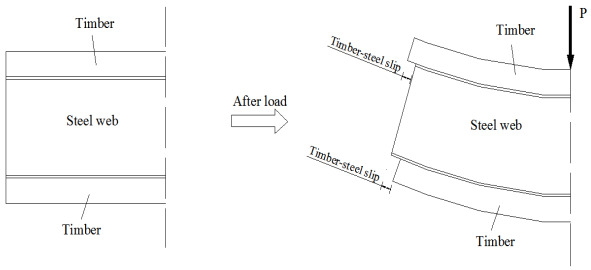

(a) Schematic diagram of slips

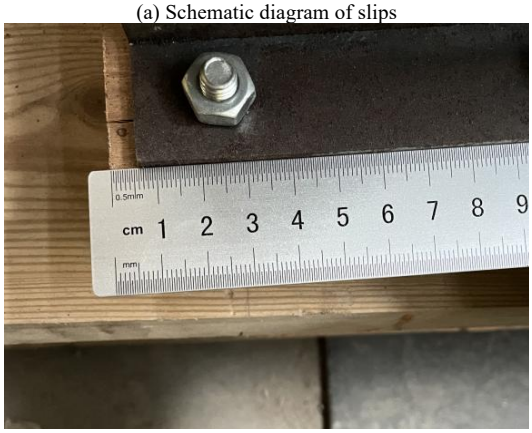

(b) Slip of upper flange relative to steel web

(c) Slip of lower flange relative to steel web

Fig. 9. Relative timber–steel slips at beam ends

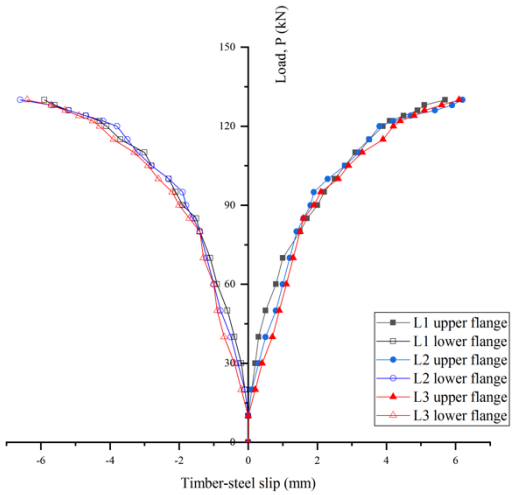

Fig. 10. Load-slip curves

The curves show that the relative slips between flange timber and web steel at the beam ends of three composite beams exhibit the same variation trends, all of which increase gradually with the increasing load. After the load exceeded 70% of the ultimate load, the increase in slip became more obvious. This phenomenon can be attributed to the yielding of bolts caused by excessive deformation, thus remarkably decreasing the anti-slip stiffness at the interface. At this point, the integrity of composite beams was reduced, and the flanges and web begin to work independently.

4.6 Calculation of deflections and bearing capacities

4.6.1 Basic assumptions

Considering the obvious relative slip effect of timber and steel in the present tests, the deflection and bearing capacityt calculated by conventional methods, which ignore the slip effect, are highly erroneous. Hence, the slip effect was considered in all the deflection and bearing capacity calculations of the composite box beams in the present study. For computational convenience, the following assumptions are made:

(1) Considering that the thickness of timber in the compressive zone entering the yield stage is very small during specimen failure, the plasticity at the upper edge of web steel is also small. Besides, the timber presents brittle failure under tension, without obvious plasticity. Thus, during failure of the specimens, the bending deformation still satisfies the plane section assumption. In other words, the plastic deformations of compressed flanges and web upper steel are ignored, as shown in Figure 11(a).

(2) Based on the findings of Fu Guo et al. [26] and He Guichao et al. [27], this study assumes that the actual limit state of composite box beams is a linear superposition of the limit state ignoring slip and the additional effects caused by slip. Figure 11(b) depicts the superposition pattern.

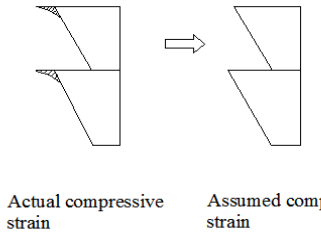

(a) Compressive strain assumption

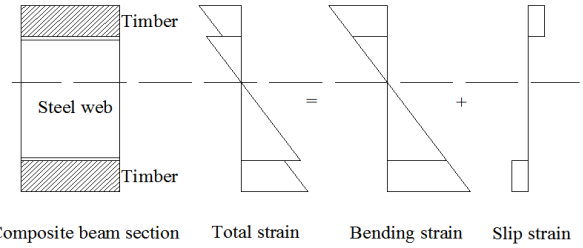

(b) Strain superposition pattern

Fig.11. Schematic of section compressive strain assumption and superposition pattern

4.6.2 Mid-span deflections

Based on the foregoing assumption (1), the stiffness can be calculated using the following equation by regarding composite box beams approximately as an ideal elastic material under the limit state ignoring slip:

$$EI = E_s I_s + E_w I_w \tag{6}$$

where E represents the elastic modulus of composite beam, I denotes the moment of inertia of composite beam section about its centroid, E_s and E_w represent the elastic moduli of steel and timber, and Is and Iw are the moments of inertia of steel and timber about centroid, respectively.

When ignoring slips, the mid-span deflection Δ_1 of simply supported composite box beam is calculated as follows:

$$\Delta_1 = \beta_s \frac{PaL^2}{48EI}\left(3-4\alpha^2\right) \tag{7}$$

where a denotes the distance from loading point to proximal support, and α refers to the ratio of a to beam span, where $\alpha = a/L$. Besides, β_s is the deformation development coefficient of timber–steel composite beams, whose value can be 1.2 if $L \leq 3$m.

By substituting Equation (6) into Equation (7), the mid-span deflection of simply supported composite box beam can be obtained under the limit state that ignores slip.

The additional deflection of timber–steel composite beam caused by slip was calculated based on the reduced stiffness method proposed by Professor Nie Jianguo of Tsinghua University [28]. When the two points were loaded symmetrically, the additional deflection Δ_2 was calculated using the following formulas:

$$\Delta_2 = \frac{\beta P}{2\mathrm{h}}\left(\frac{L}{2} - \mathrm{s} - \frac{\mathrm{e}^{-\mathrm{mb}}}{\mathrm{m}}\right)$$
$$\beta = \frac{\mathrm{h}P}{2KA_1}$$
$$m = \sqrt{\frac{KA_1}{E_s I_0 \mathrm{p}}} \quad (8)$$
$$A_1 = \frac{I_0}{A_0} + \left(\frac{\mathrm{h}}{2}\right)^2$$
$$\frac{1}{A_0} = \frac{1}{A_s} + \frac{\mathrm{n}}{A_t}$$
$$I_0 = I_s + I_t / \mathrm{n}$$

where K represents the stiffness coefficient of bolts, $K = 0.66 n_s V_u$ (n_s and V_u denote the number of bolts in the same section and the ultimate shear bearing capacity of individual bolts, respectively), P refers to the total external load, p denotes the bolt pitch, and s respectively represent the span length and the distance from loading point to mid-span, h denotes the section height, A_0 represents the area of transformed section, and A_s and A_t represent the sectional areas of steel and timber, respectively. I_0, I_s and I_t denote the moments of inertia of transformed section, steel, and timber, respectively, and n is the elastic modulus ratio of steel to timber.

The overall deflection of composite beam is as follows:

$$\Delta = \Delta_1 + \Delta_2 \quad (9)$$

The deflection calculations of the composite beams were compared with the corresponding test results, as shown in Table 5.

Table 5. Comparison of the calculated versus experimental deflection values

Specimen No.	Δ (mm)	Δ' (mm)	Δ / Δ'
L1	64.4	60.8	1.06
L2	64.4	66.2	0.96
L3	64.4	61.2	1.05
$\bar{L}$	64.4	62.73	1.027

Note: $\bar{L}$ represents average values of composite box beams, and Δ' denotes the mid-span deflection values measured by tests.

Comparison results reveal that the calculated and experimental values of mid-span deflection for the composite box beams agree well with each other, in which the errors are within 10%, which meet the demands of practical engineering applications.

4.6.3 Bending capacities

Based on the foregoing assumption (2), when slip was disregarded, the bearing capacities of composite box beam can be solved according to the superposition principle. Their computational formulas are as follows:

$$M = M_s + M_w$$
$$M_s = \gamma f_y W_s \quad (10)$$
$$M_w = \sigma_w W_W$$

where M represents the ultimate bending capacity of composite box beams ignoring the slip effect, M_s and M_w denote the bending capacities of steel and timber, W_s and W_w denote the sectional resistance distances of the beam steel and timber, respectively, σ_w denotes the parallel-to-grain compressive strength of steel (value assigned according to the material performance test results), f_y denotes the yield strength of steel, and γ refers to the plastic development coefficient of steel. In the present tests, the plastic development of steel was small, and the plastic deformation of steel was ignored according to the assumption (1). Thus, γ was set to 1.0 following the *Design Code for Steel Structures*.

The additional bending moment M_e generated by the slip effect was calculated as follows:

$$M_e = N_{cw} y_1 + N_{tw} y_2$$
$$N_{cw} = E_w \varepsilon_s t b_1 \quad (11)$$
$$N_{tw} = E_w \varepsilon_s t b_2$$

where N_{cw} and N_{tw} represent the resultant forces of compressive and tensile stresses produced by slips of top and bottom timber, and y_1 and y_2 denote the distances from N_{cw} and N_{tw} to the section central axis, respectively.

For the computational convenience of slip effect, the concept of relative timber–steel slip strain is introduced to represent the relative dislocation per unit length at the timber–steel interface, while the integral of the relative slip strains along the beam length is precisely the final slip. In formula (11), ε_s denotes the relative slip strain. Considering the excessively large difference between the ultimate compressive strengths of timber and steel, the timber already yielded or even reached the ultimate compressive strain when the steel reached the yield. Thus, in the present study, the difference between the yield strain of steel and the ultimate compressive strain of timber are adopted, in which $\varepsilon_s = \frac{f_y}{E_s} - \frac{\sigma_w}{E_w}$. Based on the calculation, the integral of ε_s along the beam length is 5.88 mm, which approximates the maximum slip (6mm) measured by the tests. This finding indicates that the relative slip strain ε_s is in line with the actual situation.

Accordingly, the actual ultimate bearing capacity of the composite box beams is as follows:

$$M_u = M - M_e \quad (12)$$

Table 6 details the comparisons of experimental results (M_u') versus theoretical calculations (M_u) for the ultimate bearing capacity of the composite box beams. The calculations of ultimate bearing capacity are in good agreement with the experimental values, in which the errors were all being less than 10%. The additional effects generated by slip reduced the bearing capacity by 24.9%. Clearly, the interface slip effect of composite box beams is non-negligible in practical engineering.

Table 6. Theoretical versus experimental values of ultimate bearing capacity

Specimen	M (kN·m)	M_e (kN·m)	M_u (kN· m)	M_e / M	$M_u^{'}$ (kN· m)	d_M (%)
L1	42.5	10.6	31.9	24.9%	33.7	5.6
L2	42.5	10.6	31.9	24.9%	32.6	2.2
L3	42.5	10.6	31.9	24.9%	33.4	4.7
$\overline{L}$	42.5	10.6	31.9	24.9%	33.23	4.2

Note: $\overline{L}$ represents average values of three composite box beams, and d_M denotes the errors between calculated and experimental values, $d_M = \left| \frac{M_u^{'} - M_u}{M_u} \right|$.

5. Conclusions

To explore the bending behavior of timber-steel composite box beams and reveal their flexural failure mechanisms, the results of bending loading tests between timber-steel composite box beams and plywood box beam were theoretically and experimentally analyzed respectively. The following conclusions could be drawn:

1) The failure modes of composite box beams are all typical tensile and compressive failures. The wood fibers of bottom plates underwent brittle fracture under tension, while the timber of top plates was crumpled because of compressive yielding. These conditions are accompanied by local longitudinal shear cracks and buckling of steel upper edges. For the plywood box beam, shear cracks were generated in the middle of web, resulting in failure. The webs of the composite box beams are made of steel with high shear resistance, so that the flange timber can fully exert its tensile and compressive properties. Thus, this composite mode is reasonable and superior.

2) In comparison with the plywood box beam, the ultimate bending capacities of the composite beams increased by 30.3% on average. Considering the slip effect with bolted connection, the initial stiffness of the composite beams was slightly reduced, although their ductility is better than that of plywood box beam. The lateral distribution analysis of flange strains show that evident shear lag effect is present in both types of beams.

3) Considering the unsound and unsystematic computational theory for the timber-steel composite structures, the mid-span deflection and ultimate bearing capacity of timber-steel composite box beams are calculated based on the computational method for steel-concrete composite beams. The calculations are consistent with the test results, in which all errors were less than 10%, which can meet the demands of practical engineering applications.

The present study reveals the failure mechanisms and flexural mechanical properties of timber-steel composite box beams through bending loading tests combined with theoretical analysis. The theoretically calculated deflection and bearing capacity values are also in good agreement with the experimental results, and these findings can provide a certain reference for the later research of timber-steel composite structures. Considering the shortcomings of this study, such as small number of specimens, no parametric variation, the mechanical behavior needs to be further studied. Hence, in future research, the factors affecting the bearing capacity and shear performance of composite beams should be investigated. Besides, on the basis of more experimental studies, the computational formulas for deflection and bearing capacity, which are more suitable for practical applications, can be proposed.

Acknowledgements

This work was supported by the follow-up program of the Chinese International Science and Technology Cooperation Special Program: Research on the Fabrication Technologies of Modern Plywood Structures (9010263203077).

References

1. Yang, T., Wang, J. J., "Experimental research on flexural bearing capacity of larch glulam T-beam". *Journal of Central South University of Forestry & Technology,* 39(5), 2019, pp.124-131.
2. Li , J. Z ., Wang, J. J., Peng, Q., "Experimental Study on the Shear Performance of T-section Beams of Glued Timber". *Journal of Engineering Science and Technology Review*, 13(6), 2021, pp.175-186.
3. Kazimierz, F., Konrad, R., "Experimental investigations of load-bearing capacity of composite timber-glass I-beams". *Archives of Civil and Mechanical Engineering*, 18(3), 2018, pp.956-964.
4. Wang, H. C., Du, H., Hu, X., M., Zhang, B., "Calculation method of shear stiffness for inclined cross screws connectors in glulam-concrete composite beams". *Journal of Building Structures*, 40(S1), 2019, pp.347-353.
5. Khan, M. S., Prof, N. S., Pawar, Y. P., "Timber–steel-Composite Beams for Framed Structure". *International Journal of Engineering Research & Technology*, 8(6), 2019, pp.1330-1335.
6. F. Nouri, H.R. Valipour, M.A. Bradford, "Structural behaviour of steel-timber composite (STC) beam-to-column connections with double angle web cleats subjected to hogging bending moment". *Engineering Structures,* 192, 2019, pp.1-17.
7. Keipour, N., Valipour, H. R., Bradford, M. A. , "Steel-timber composite beam-to-column joints: effect of connections between timber slabs". *Journal of Constructional Steel Research*, 151, 2018, pp.132-145.
8. Awaludin, A., Rachmawati, K., Aryati, M. , AD Danastri, "Development of cold formed steel – timber composite for roof structures: compression members". *Procedia Engineering*, 125, 2015, pp.850-856.
9. Mark A. Bradford, Amirhossein, H., Hamid R, V., Stephen J. F., "Sustainable Steel-timber Joints for Framed Structures". *Procedia Engineering*, 172, 2017, pp. 2-12.
10. Hassanieh, A., Valipour, H. R., Bradford, M. A., "Experimental and numerical study of steel-timber composite (STC) beams". *Journal of Constructional Steel Research*, 122, 2016, pp.367-378.
11. Hassanieh, A., Valipour, H. R., Bradford, M. A., "Load-slip behaviour of steel-cross laminated timber (CLT) composite connections". *Journal of Constructional Steel Research*, 122, 2016, pp.110-121.
12. Hassanieh, A., Valipour, H. R., Bradford, M. A., "Experimental and analytical behaviour of steel-timber composite connections". *Construction and Building Materials*, 118, 2016, pp.63-75.
13. A. Ataei, A.A. Chiniforush, M. Bradford, H. Valipour, "Cyclic behaviour of bolt and screw shear connectors in steel-timber composite (STC) beams". *Journal of Constructional Steel Research,* 161, 2019, pp.328-340.
14. Fujita, M., Iwata, M., "Bending Test of the Composite Steel-Timber Beam". *Applied Mechanics and Materials*, 351-352, 2013,

pp. 415- 421.
15. Wang,J.,R., Duan, S., W., He, J., W., Wang, Z., F., "Experimental Analysis of Eccentric Compression Performance of Larch Timber–steel Composite Columns". *Advances in Civil Engineering*, 2019, 2019, pp.1-17.
16. Wang, J., J., Lu, Y., Lei, Y., Wang, H., L., "Comparative study on flexural behavior of steel–timber composite beams and glued timber i-beams". *Journal of Engineering Science and Technology Review*, 13(6), 2020, pp.175-186.
17. Duan, S., W., Zhou, W., Z., Liu, X., L., Yuan, J., Wang, Z., F., "Experimental Study on the Bending Behavior of Steel-Timber Composite Beams". *Advances in Civil Engineering*,2021,2021,pp.1-12.
18. Gao, Y., M., "*Research on CLT Steel-wood Composite Bridge Deck System*". Master thesis of Chang'an University, China, 2010, pp.59-60.
19. Chen, A., J., Peng, R., X., He, G., J., Wang, J., J., "Shear Behavior of Bolted Connections with Steel Plate in Assembled Timber Structures". *China Journal of Highway and Transport*, 31(12), 2018, pp.59-70.
20. Chen, A. G., Li, D. H., Fang, C., Zheng, Q. G., Xing, J. H., "Experimental study on flexural behavior of H-shaped steel-timber composite beams". *Journal of Building Structures*, 37(S1), 2016, pp.261-267.
21. Yao, X., F., "*Study on Bending Mechanical Behavior of Steel-Timber Composite Beam* ". Master thesis of Dalian University of Technology, China, 2017, pp.60-61.
22. *Design Handbook for Timber Structures* Editorial committee, *"Design Handbook for Timber Structures"*. Beijing, China Architecture & Building Press, 2005, pp.43-48.
23. Xu, B., H., Cai, J., "State-of -the art in strength criteria for wood". *China Civil Engineering Journal*, 48(1), 2015, pp.64-73.
24. Xu, G., "*Experimental study on shear lag effect in simply supported concrete box girder*". Master thesis of Huaqiao University, China, 2016, pp.17-58.
25. Li, P., "*Experimental Research on Shear Lag Effect of Steel-Concrete Composite Box Girder*". Master thesis of Suzhou University of Science and Technology, China, 2009, pp.44-45.
26. Fu, G., "*Experiments and Theoretic Research on Steel-Concrete Composite Beams Considering Interface Slip and Uplift*". Doctoral Dissertation of Xi'an University of Architecture and Technology, China, 2008, pp.50-66.
27. He, G., C., Zhou, L., Y., "Energy variational method of shear deformation and slip effect of steel-concrete composite box beam". *Journal of Central South University (Science and Technology)*, 43(11), 2012, pp.4433-4438.
28. Nie, J., G., Shen, J., M., Yu, Z., W., "A Reduced Rigidity Method for Calculating Deformation of Composite Steel-Concrete Beams". *China Civil Engineering Journal,* 28(6), 1995, pp.11-17.